Protein Conformational Changes in Tetraheme Cytochromes Detected by FTIR Spectroelectrochemistry: *Desulfovibrio desulfuricans* Norway 4 and *Desulfovibrio gigas* Cytochromes c_3

Daniela D. Schlereth,[‡,§] V. M. Fernández,[∥] and Werner Mäntele*[,‡]

Institut für Biophysik, Albertstrasse 23, D-79104 Freiburg, Germany, and Instituto de Catálisis (CSIC), Campus Universitario de la Universidad Autónoma, Cantoblanco, 28049 Madrid, Spain

Received December 7, 1992; Revised Manuscript Received April 13, 1993

ABSTRACT: The conformational change coupled to the redox processes of two tetraheme cytochromes c_3 from bacteria of the genus *Desulfovibrio* have been studied by UV–vis and FTIR difference spectroscopy combined with protein electrochemistry. Two pairs of equivalent hemes were found in *Desulfovibrio desulfuricans* Norway 4 cytochrome c_3 by UV–vis spectroelectrochemical redox titration in an optically transparent thin-layer electrochemical cell. In contrast to this, *Desulfovibrio gigas* cytochrome c_3 showed a UV–vis difference spectrum for the highest potential heme different from that of the others. The redox titrations were monitored by FTIR difference spectroscopy using the same spectroelectrochemical cell. They show that in both cytochromes the overall redox process from the fully oxidized (III_4) to the fully reduced oxidiation state (II_4), $III_4 \Leftrightarrow II_4$, proceeds via an intermediate oxidation stage (III_2II_2) which is formed after the second electron uptake. The small amplitude of the difference signals in the reduced-minus-oxidized FTIR difference spectra obtained for the overall redox process in both *Desulfovibrio* cytochromes indicates a very small conformational change induced by the redox transition. Nevertheless, by application of potential steps from the fully oxidized or reduced form to the midwave potential (as obtained from the UV–vis redox titrations), the reduced-minus-oxidized IR difference spectra corresponding to the intermediate redox transitions ($III_4 \Leftrightarrow III_2II_2$ and $III_2II_2 \Leftrightarrow II_4$) were obtained, reflecting separately the contributions of the high- and low-potential heme pairs to the overall redox-induced conformational change. The overall redox process and both intermediate redox transitions were fully reversible. In the spectral region between 1500 and 1200 cm^{-1} the IR difference spectra of both cytochromes show several signals previously observed in the reduced-minus-oxidized IR difference spectra of spinach cytochrome b_{559} and iron–protoporphyrin IX–bis(imidazole) model compounds [Berthomieu, C., Boussac, A., Mäntele, W., Breton, J., & Nabedryk, E. (1992) *Biochemistry 31*, 11460–11471]. Moreover, Raman spectra of *Desulfovibrio vulgaris* cytochrome c_3 and cytochrome b_5 show signals attributed to Raman active heme skeletal modes at nearly the same positions [Kitagawa, T., Kyogoyu, Y., Izuka, T., Ikeda-Saito, M., & Yamanaka, T. (1975) *J. Biochem. 78*, 719–728], thus allowing their assignment to signals arising from heme vibrational modes. Comparatively strong IR difference signals at 1618 cm^{-1}, which are tentatively assigned to phenylalanine residues, were found in *D. desulfuricans* cytochrome c_3. In the spectra of *D. gigas* cytochrome c_3, IR signals at 1614 cm^{-1} were detected only for the first redox transition ($III_4 \Leftrightarrow III_2II_2$). The IR reduced-minus-oxidized difference spectra of *D. gigas* cytochrome c_3 corresponding to both redox transitions ($III_4 \Leftrightarrow III_2II_2$ and $III_2II_2 \Leftrightarrow II_4$) show a small and sharp signal at 1512 cm^{-1} which is tentatively assigned to tyrosine residues.

Cytochromes c_3 constitute a class of multiheme proteins which act as electron carriers in the sulfate-reducing bacteria of the genus *Desulfovibrio* (DerVartanian & Le Gall, 1974). In the metabolism of these bacteria, molecular hydrogen enters the system via a hydrogenase which specifically reduces cytochrome c_3 (cyt-c_3),[1] which in turn reduces ferredoxin (Postgate, 1981). The cyt-c_3 molecule can be described as a short single polypeptide chain (MW about 13 000) which contains four bis(histidyl)porphyrin rings bound by two thioether linkages (Dobson et al., 1974; Haser et al., 1979; Pierrot et al., 1982; Higuchi et al., 1984). These proteins are autoxidizable and exhibit strongly negative redox potentials of around −300 mV *vs* SHE (Le Gall et al., 1965; Yagi & Maruyama, 1971; Bianco & Haladjan, 1981).

A very poor homology is found among the available amino acid sequences of cytochromes c_3 from different *Desulfovibrio* species. In spite of this variation, Haser et al. (1979) proposed that the heme environments as well as their geometrical arrangement in the molecule found in *Desulfovibrio desulfuricans* Norway 4 (D.d.N.) cyt-c_3 could be considered as a general model for all cytochromes c_3. The comparison between the crystal structures of D.d.N. (Haser et al., 1979; Pierrot et al., 1982), D.v.M. (Higuchi et al., 1984), and *Desulfovibrio vulgaris* Hildenborough (D.v.H.) cytochromes c_3 (Morimoto et al., 1991) supports this hypothesis.

‡ Institut für Biophysik.

§ Present address: Lehrstuhl für Allgemeine Chemie und Biochemie, Technische Universität München, Vöttingerstrasse 40, D-8050 Freising-Weihenstephan, Germany.

∥ Instituto de Catálisis.

[1] Abbreviations: cyt-c_3, cytochrome c_3; D.d.N., *Desulfovibrio desulfuricans* Norway 4; D.g., *Desulfovibrio gigas*; D.v.M., *Desulfovibrio vulgaris* Miyazaki; D.v.H., *Desulfovibrio vulgaris* Hildenborough; HP, high potential; LP, low potential; Pys, bis(4-pyridyl) disulfide; SME, surface-modified electrode; $E_{50\%}$, half-wave potential; E, redox potential; E_{pc}, cathodic peak potential; E_{pa}, anodic peak potential; $E_{1/2}$, midpoint potential; III, II, heme in the oxidized or reduced state, respectively; red-ox, reduced minus oxidized.

0006-2960/93/0432-9199$04.00/0

As a general feature, these molecules contain four nonequivalent hemes nonsymmetrically arranged, highly exposed to the solvent but still partially shielded by some aromatic amino acid residues. Moreover, some of these aromatic residues are thought to be involved in the intramolecular (Pierrot et al., 1982; Park et al., 1991) and intermolecular (Stewart et al., 1988) electron-transfer reactions. A small conformational change induced after reduction of the redox centers has been suggested for various *Desulfovibrio* cyt-c_3 from *africanus* (Singleton et al., 1979), *desulfuricans* Norway (Pierrot et al., 1982), and *vulgaris* Miyazaki strains (Tabushi et al., 1983; Yagi, 1984; Gayda et al., 1987).

Kinetic studies of the nonenzymatic chemical reduction of D.v.H. and D.d.N. cyt-c_3 have shown that the reduction process exhibits biphasic kinetics, with a slow step after the uptake of the third electron (Capellière-Blandin et al., 1986). Similar biphasic kinetics involving one fast heme and three slow hemes has been found for the D.g. cyt-c_3 (Catarino et al., 1991). The same phenomenon was found for the enzymatic reduction of D.v.M. cyt-c_3 with a partially oxygenated hydrogenase (Yagi, 1984). Intermediate oxidation stages with different optical, CD, and ESR spectral properties have been found in D.d.N. (Cammack et al., 1984) and D.v.M. cyt-c_3 (Tabushi et al., 1983; Yagi, 1984; Gayda et al., 1987).

According to X-ray data, the molecule of D.d.N. cyt-c_3 folds in two domains joined by the segment [Phe-72–Arg-73], which contains the hemes I and III (H_I and H_{III}) separately. [The subindexes follow the heme assignment in the crystal structure given by Haser et al. (1979).] These domains are separated by a large groove which accommodates H_{II} and H_{IV}; H_{II} is anchored in the only α-helical segment which supplies also one axial ligand for H_I (Pierrot et al., 1982). According to the heme–heme distances found in the crystal, the redox cluster could be considered as being formed by two heme pairs, namely (H_I, H_{IV}) and (H_{II}, H_{III}) (Haser et al., 1979; Pierrot et al., 1982). The same arrangement was found in the structure of D.v.M. cyt-c_3 (Higuchi et al., 1984). However, the assignment of the individual heme redox potentials to the hemes in the crystal structure is not yet well established (Haser et al., 1979; Pierrot et al., 1982; Capellière-Blandin et al., 1986; Dolla et al., 1987). More recently, on the basis of ESR studies, the sequence of redox potentials $E_{II} < E_I < E_{IV} < E_{III}$ was proposed by Guigliarelli et al. (1990).

The X-ray data available from cytochromes c_3 provide an accurate picture of the arrangement of the hemes as well as of the amino acids surrounding the hemes and interacting with redox partners. However, the presently available information on redox-induced conformational changes can only be considered tentative. Infrared spectroscopy is a suitable analytical tool to obtain information even on minor conformational changes. In previous work, we have used Fourier transform infrared (FTIR) difference spectroscopy combined with protein electrochemistry to analyze the conformational changes induced by the redox transitions in some heme proteins, such as cytochrome *c* (Moss et al., 1990; Schlereth & Mäntele, 1993), myoglobin, and hemoglobin (Schlereth & Mäntele, 1992).

In the work presented here, we have investigated the conformational change involved in the redox transition in D.d.N. and D.g. cyt-c_3. We have found that in both proteins the redox process proceeds via an IR-detectable intermediate oxidation stage involving two hemes. From the whole sequence of electrochemical events ($III_4 \Leftrightarrow III_3II_1 \Leftrightarrow III_2II_2 \Leftrightarrow III_1II_3 \Leftrightarrow II_4$), we were able to obtain reduced-minus-oxidized (red-ox) IR difference spectra for two bielectronic redox steps, namely $III_4 \Leftrightarrow III_2II_2 \Leftrightarrow II_4$, involving the high-potential (HP) and the low-potential (LP) heme pairs, respectively; each difference spectrum had nearly the same signal amplitude for heme and amide I modes. This would imply that each heme pair acts in a concerted manner, and the overall redox-induced conformational change could be described as a movement of the polypeptide backbone in two half-steps, each one involving half of the whole molecule. Even though we cannot deduce from our experiments the assignment of an individual redox potential to a particular heme, it appears that in each bielectronic electrochemical process ($III_4 \Leftrightarrow III_2II_2$ and $III_2II_2 \Leftrightarrow II_4$) only one domain of the molecule is involved, in agreement with the heme assignment proposed by Guigliarelli et al. (1990).

MATERIALS AND METHODS

(1) Sample and Electrode Preparation. The OTTLE cell suitable for UV–vis and IR spectroscopy of proteins in aqueous solvents has been described previously (Moss et al., 1990) and used with minor modifications (Baymann et al., 1991). As an essential feature of this cell, the protein solution forms a 10–15-μm layer on a 70% transparent gold grid working electrode (Buckbee-Mears, St. Paul, MN) between two CaF_2 windows, in electrical contact with a platinum foil counter-electrode and a Ag/AgCl/3 M KCl reference electrode (all of the potentials quoted in this work are referred to this electrode; add +208 mV for potentials *vs* standard hydrogen electrode).

Cytochrome c_3 (cyt-c_3) from *D. desulfuricans* Norway 4 (D.d.N.), purified following the method of Bruschi et al. (1977), was a generous gift of Prof. K. K. Rao (King's College, London). Cyt-c_3 from *Desulfovibrio gigas* (D.g.) was purified following the method of Le Gall and Forget (1978) from cells grown in the Laboratoire de Chimie Bactérienne du CNRS (Marseille). The samples were dialyzed against a 50 mM, pH 7.1, phosphate buffer, containing 100 mM $LiClO_4$ as supporting electrolyte, and afterward concentrated in an ultrafiltration cell (Amicon, Witten). For measurements at different pH values, phosphate buffers of pH 6.1 and 8.3 were used, and for more alkaline pH values small amounts of KOH were added. The concentration of the samples was determined spectrophotometically from the absorbance of the α band in the reduced protein, using as molar extinction coefficients ϵ_{553} = 130 and 120 mM cm^{-1} for D.d.N. and D.g. cyt-c_3, respectively (Bianco & Haladjan, 1979; Le Gall & Forget, 1978). The purity index as determined by the absorbance ratio $[A_{553}(red) - A_{570}(red)]/A_{280}(ox)$ (Bruschi et al., 1977) was about 3 for both proteins. Samples in ^2H_2O were prepared by dilution of the previously concentrated sample in a 50 mM phosphate–^2H_2O buffer, pD 7.5, containing 100 mM $LiClO_4$, equilibrium for 48 h, and reconcentration to 1–5 mM.

Electrochemistry of D.d.N. cyt-c_3 was performed using gold grid surface-modified electrodes (SMEs). The working electrode was freshly modified before each experiment by soaking the grid for 10 min either in a 0.8 mg/mL acidic solution of bis(4-pyridiyl) disulfide (Pys) (Taniguchi et al., 1982a,b) or in a 10 mg/mL aqueous solution of L-cysteine (di Gleria et al., 1986). For D.g. cyt-c_3 either the bare gold grid electrode or the grid modified with a 10 mg/mL aqueous solution of cystamine chlorhydrate (Hill & Lawrance, 1989) was used. All of the surface modifiers were purchased from Sigma and used without further purification. To avoid the presence of modifiers in the protein solutions, the electrodes were thoroughly rinsed with distilled water before use.

(2) UV–Vis Spectroscopy and Electrochemistry. The equipment used for chronoamperometry, cyclic voltammetry,

and coulometry was constructed in our laboratory according to standard designs. UV–vis spectra were recorded on a remodeled Cary 14 spectrophotometer or on a single-beam spectrophotometer built to our design. Both spectroscopy and electrochemistry were controlled through interfaces from data acquisition and treatment software (MSPEK) developed in our laboratory by D. Moss and S. Grzybek. Titration curves were evaluated using standard least-squares fitting software.

The equilibration time of the samples at a constant applied potential was that required to reach a constant value in the time-dependent absorbance change of the Soret difference band at 420 (D.d.N. cyt-c_3) or 421 nm (D.g. cyt-c_3). Titration curves were obtained at room temperature and different pH values, using the different electrodes with protein samples at concentrations between 1 and 3 mM.

(*3*) *FTIR Difference Spectroscopy.* All of the IR difference spectra shown in this work were recorded at 5 °C on a Bruker IFS 25 FTIR spectrophotometer equipped with a MCT detector of selected sensitivity. The FTIR spectrophotometer was modified to allow the measuring beam of the single-beam spectrophotometer for visible light to pass coaxially through the sample, thus allowing simultaneous recording of the UV–vis and IR spectra. IR difference spectra were calculated from single-beam spectra (each one was the average of 128 scans at 3 scans/s) I_1 and I_2 of the sample equilibrated at the different potentials by forming $A = \log(I_2/I_1)$. To obtain a high signal-to-noise ratio, the difference spectra shown in this work are the result of an averaging of several difference spectra obtained after successive electrolysis cycles. No baseline subtractions or weighted subtractions of buffers were performed.

RESULTS

(*1*) *Electrochemistry and UV–Vis Difference Spectroscopy.* (*1.1*) *D. desulfuricans Norway 4* (*D.d.N.*) *Cytochrome* c_3. Figure 1A shows the titration curve obtained with a sample of D.d.N. cyt-c_3 with the bis(4-pyridyl) disulfide surface-modified electrode (Pys–SME). The time required for the equilibration of the sample at each potential step was 50 s. The superposition of both reductive and oxidative titration curves indicates that the redox process is perfectly reversible. The titration curve shows two electrochemical processes with half-wave potentials at –370 and –550 mV. The first process leads to change in the Soret difference band of ≈26% of the overall absorbance change and can be attributed to the oxidoreduction of the less exposed heme (H_{III}) (Haser et al., 1979; Pierrot et al., 1982). Thus, the second process must involve the three low-potential hemes (H_I, H_{II}, and H_{IV}). The half-maximum value of the amplitude of the Soret difference band is reached at $E_{50\%}$ = –520 mV.

The titration curve in Figure 1A can be fitted with a Nernst curve for an electrochemical process with four noninteracting components of equal amplitude with individual macroscopic redox potentials at $E_{(III)}$ = –371 mV; $E_{(IV)}$ = –505 mV; $E_{(I)}$ = –542 mV and $E_{(II)}$ = –575 mV [individual heme redox potentials assignment as in Guigliarelli et al. (1990)]. The same results were obtained with cysteine–SMEs (data not shown). The cyclic voltammogram recorded with the Pys–SME (Figure 2A) shows two waves corresponding to two reversible and diffusion-controlled electrochemical processes with midpoint potentials at $(E_{1/2})_1$ = –336 and $(E_{1/2})_2$ = –532 mV.

The titration of the α band shows that the redox transition from the two high-potential (HP) to the low-potential (LP) hemes is coupled with a shift of the alpha band maximum from 554 to 553 nm. Figure 3A shows the UV–vis reduced-minus-oxidized (red-ox) difference spectra of both HP and LP hemes obtained after potential steps of 0 → –520 and –520 → –650 mV were applied. The absorbance maxima of the LP hemes ($420_{(red)}$, $552_{(red)}$, and $403_{(ox)}$ nm) appear at slightly shorter wavelengths than those of the HP hemes ($421_{(red)}$, $554_{(red)}$, and $406_{(ox)}$ nm).

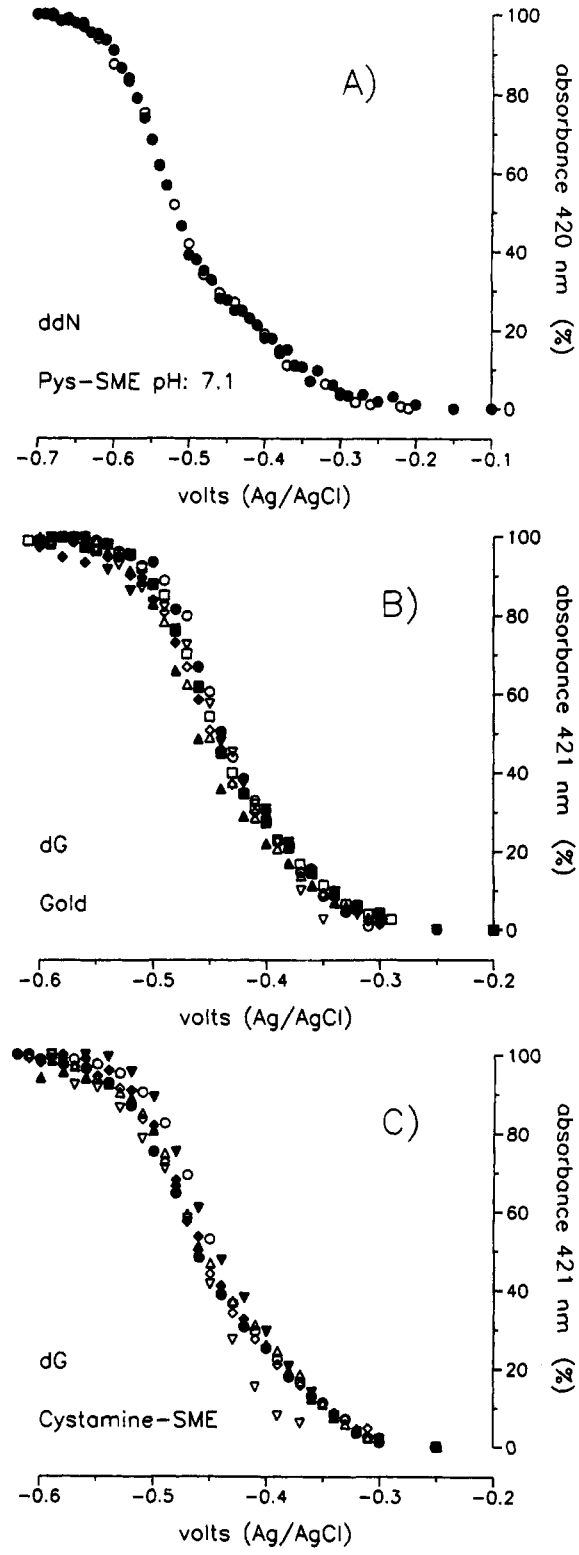

FIGURE 1: Reductive (solid symbols) and oxidative (open symbols) redox titrations monitored by UV–vis difference spectroscopy: (A) D.d.N. cyt-c_3, pH 7.1, at the Pys–SME; (B) D.g. cyt-c_3, pH 6.1 (○), 7.1 (□), 8.3 (△), 9.8 (◇), and 11.4 (▽) at the bare gold electrode; (C) D.g. cyt-c_3 at the cystamine–SME [conditions as in (B)].

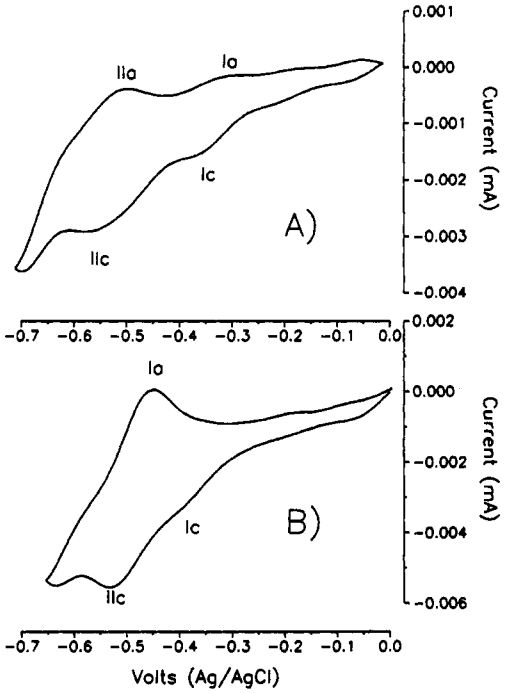

FIGURE 2: Cyclic voltammograms of (A) D.d.N. cyt-c_3 and (B) D.g. cyt-c_3. Conditions: pH 7.1; sweep rate 1 mV/s.

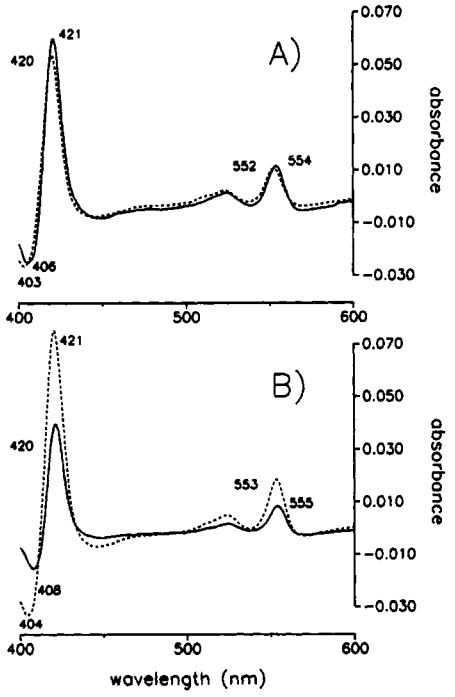

FIGURE 3: UV–vis difference spectra of the P (—) and LP (- - -) hemes of (A) D.d.N. cyt-c_3 and (B) D.g. cyt-c_3.

(1.2) D. gigas (D.g.) Cytochrome c_3. Figure 1B shows the titration curves obtained with 1 mM D.g. cyt-c_3 at the bare gold electrode at different pH values between 6.1 and 11.4 (for details, see legend). Independent of the pH value, full equilibration of the cell was achieved 50 s after the potential step.

At the pH values investigated, both reductive and oxidative titration curves could be superposed and show only one redox process with a half-wave potential at $E_{50\%}$ = –460 mV.

In contrast to D.d.N. cyt-c_3, the titration curves obtained with D.g. cyt-c_3 could not be fitted with a Nernst curve composed of four noninteracting components. Nearly the same curves were obtained with the cystamine–SME (Figure 1C). However, with the cystamine–SME at alkaline pH above 9.8, the reductive and the oxidative titration curves were not perfectly superimposable (Figure 1C).

The cyclic voltammogram recorded with the gold electrode (Figure 2B) shows two cathodic waves at E_{pc}(I) = –405 mV and E_{pc}(II) = –530 mV and only one anodic wave at E_{pa} = –450 mV. Cyclic voltammograms recorded under different pH conditions were nearly identical.

It may be important to note that prolonged storage of the protein at 4 °C resulted in a shift of the redox potentials toward 100-mV more negative values, as well as in the loss of the heme–heme interactions. With an aged sample of D.g. cyt-c_3, we have obtained titration curves with a slight hysteresis in the oxidation process which could be fitted by a Nernst curve with four noninteracting components and individual macroscopic redox potentials at –437, –528, –577, and –596 mV (data not shown).

In analogy to the behavior of D.d.N. cyt-c_3, the titration of the α band shows a shift of the maximum from 555 to 553 nm at –410 mV. Upon application of separate potential steps of 0 → –410 mV and –410 → –600 mV, it is possible to obtain the UV–vis red-ox difference spectra corresponding to one HP heme and the three LP hemes (Figure 3B). The absorbance maxima of the LP hemes appear at $421_{(red)}$, $553_{(red)}$, and $404_{(ox)}$ nm, whereas those of the HP heme appear at $420_{(red)}$, $555_{(red)}$, and $408_{(ox)}$ nm.

(2) FTIR Difference Spectroscopy and IR Band Assignment. (2.1) D. desulfuricans Norway 4 (D.d.N.) Cytochrome c_3. (2.1.1) Total FTIR Difference Reduced-minus-Oxidized Spectrum: Overall Oxidoreduction Process from the Fully Oxidized to the Fully Reduced Oxidation State ($III_4 \Leftrightarrow II_4$). Figure 4A shows the red-ox FTIR difference spectra of D.d.N. cyt-c_3 at pH 7.1 obtained with the Pys–SME in ^1H_2O (solid line) and ^2H_2O (dotted line). After equilibration of the sample at 0 mV and recording of the single-beam spectrum of the fully oxidized sample (III_4), the potential was switched to –650 mV, and the single-beam spectrum of the fully reduced protein (II_4) was recorded after 100 s of equilibration. The IR red-ox difference spectra corresponding to the electrochemical process ($III_4 \Leftrightarrow II_4$) shown in Figure 4A were obtained by subtraction of these two single-beam spectra. Restoration of the applied potential to 0 mV for 50 s led to the complete reoxidation of the sample, and an oxidized-minus-reduced IR difference spectrum was obtained (data not shown), which was the exact mirror image of the spectrum shown in Figure 4A.

The spectra show several signals arising from vibrational modes of the polypeptide backbone, as well as from the porphyrin rings. The small amplitude of the spectra suggests a very small conformational change coupled to the redox transition. It may be estimated as follows: the sum of the amplitudes of the IR amide I difference signals corresponds to about a 3.5% of the total absorption of the amide I band (absorbance maximum at 1642 cm^{-1}, arising predominantly from the peptide C=O stretching vibration mode). This leads us to conclude that at most three to four peptide carbonyls are involved in the overall redox-induced conformational change in D.d.N. cyt-c_3. A similar small conformational change has been previously observed in the IR red-ox spectra of the isolated tetraheme cytochrome from *Chloroflexus aurantiacus* reaction centers (Fritz and Mäntele, unpublished data). As a consequence of this, relatively strong signals arising from heme modes can be detected which are difficult to see in the IR red-ox spectra of other heme proteins such as cytochrome *c* (Moss et al., 1990; Schlereth & Mäntele, 1993), myoglobin,

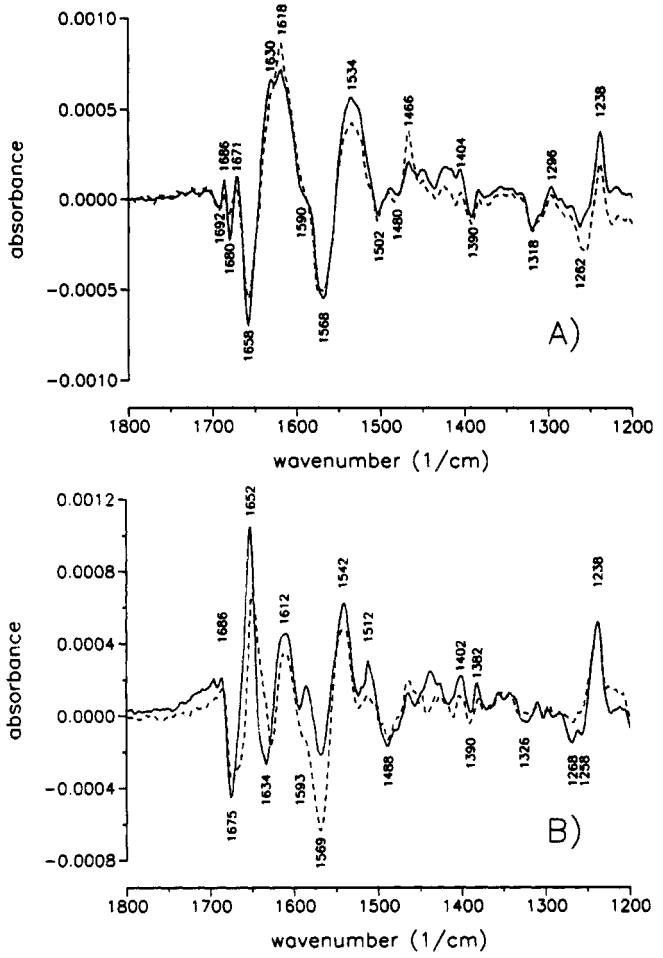

FIGURE 4: FTIR difference spectra of the global redox process ($III_4 \Leftrightarrow II_4$) in ^1H_2O, pH 7.1 (—), and ^2H_2O, pD 7.5 (- - -), of (A) D.d.N. cyt-c_3 and (B) D.g. cyt-c_3.

and hemoglobin (Schlereth & Mäntele, 1992).

The spectral region between 1670 and 1620 cm^{-1} contains signals arising from amide I C=O stretching modes. According to the different secondary structures, we tentatively assign the difference signals at 1658 (–), 1630 (+), and 1671 (+)/1680 (–) cm^{-1} to α-helical, β-sheet, and turn segments, respectively (Krimm & Bandekar, 1986). This assignment is supported by the very small shift ($<\approx 5$ cm^{-1}) of these signals in ^2H_2O (Figure 4A, dotted line). However, in this spectral region we can also expect contributions from the absorption of some amino acid side chains (Venyaminov & Kalnin, 1990; Chirgadze et al., 1975).

The weak difference signals (Figure 4A) at 1692 (–)/1686 (+) cm^{-1} could as well be assigned to amide I C=O stretching modes of β-turn segments (Susi & Byler, 1987). However, we also consider the possibility that these signals could arise from the –COOH symmetric stretching mode of protonated carboxylic acid groups. We tentatively assign these signals to heme propionic acids which are differently exposed to the solvent. We imply a close correlation between solvent exposure and the frequency, in that the less exposed absorb at higher wavenumbers. Indeed, signals at nearly the same positions are found in the IR red-ox spectra of cytochrome *c* (Moss et al., 1990; Schlereth & Mäntele, 1993), cytochrome b_{559} (Berthomieu et al., 1992), myoglobin, and hemoglobin (Schlereth & Mäntele, 1992). These signals are slightly affected by deuteration. Small shifts (less than 4 cm^{-1}) have been observed in myoglobin and hemoglobin after deuteration (Schlereth & Mäntele, 1992), and only changes in their relative amplitude were found in cytochrome *c* (Moss et al., 1990) and cytochrome b_{559} (Berthomieu et al., 1992) IR red-ox spectra. Although free propionic acid has a p*K* of about 4.5, the existence of a "high p*K*" heme propionate in cytochrome *c* which would be protonated at pH 7.0 has been observed (Hartsorn & Moore, 1989; Tonge et al., 1989). More recently, Gunner and Honig (1991) have found from electrostatic calculations of the midpoint potentials in the tetraheme cytochrome of the *Rhodopseudomonas viridis* reaction center that one of the hemes contains a high p*K* propionate. However, the molecule of D.d.N. cyt-c_3 contains 10 aspartic and 5 glutamic groups (Haser et al., 1979) which may be taken into account as possible contributors to this absorption.

The very strong positive signal at 1618 cm^{-1} could arise from the –HC=CH– stretching mode of aromatic amino acid side chains such as phenylalanine and tyrosine (Casal et al., 1988; Surewicz et al., 1987). The fact that we do not see in the spectrum the characteristic signal of phenylalanine at 1494 cm^{-1} (Venyaminov & Kalnin, 1990) could be related with the appearance of two negative signals at 1502 and 1480 cm^{-1} which could mask this signal. The strong negative signal at 1568 cm^{-1} could have contributions of the $-COO^-$ antisymmetric stretching mode of carboxylate groups from heme propionates and aspartate and glutamate residues (Venyaminov & Kalnin, 1990). However, contributions from heme modes also appear to be possible (Berthomieu et al., 1992). This band includes a shoulder at 1590 cm^{-1} which could arise from the ring vibration modes of histidines (Venyaminov & Kalnin, 1990).

The relatively high amplitude of the positive signal at 1534 cm^{-1} in comparison with the positive signal at 1238 cm^{-1} suggests that, besides the contributions of heme modes (Berthomieu et al., 1992), this signal contains also contributions from amide II modes. This could be the reason for the decrease of the amplitude of this signal in the ^2H_2O spectrum. The signals at 1238 (+), 1390 (–), 1404 (+), 1318 (–), and 1402 (–) cm^{-1} can be attributed to heme vibrational modes. The IR red-ox spectra of the iron–porphyrin–bis(imidazole) complex show signals at 1504 (–), 1405 (+), and 1239 (+) cm^{-1} and were found in the same position after deuteration (Berthomieu et al., 1992). Moreover, the Raman spectra of D.v. cyt-c_3 show signals at 1505 (1493), 1405 (1399), 1315 (1313), and 1240 cm^{-1} for the oxidized and (reduced) oxidation states (Kitagawa et al., 1975). We thus assign these signals to heme vibrational modes. A positive signal at 1466 cm^{-1} appears only in the ^2H_2O spectrum and probably arises from N–^{2}H bending modes (amide II' in ^2H_2O).

The large contributions of heme modes in the IR red-ox spectra of D.d.N. cyt-c_3 could be the reason for the very small effect of deuteration observed in the ^2H_2O spectrum besides the shift of the amide II band to 1466 (+) cm^{-1}.

(2.1.2) IR-Detectable Intermediate Oxidation Stages Corresponding to the Bielectronic Redox Processes $III_4 \Leftrightarrow III_2II_2$ and $III_2II_2 \Leftrightarrow II_4$. Following a reductive redox titration of D.d.N. cyt-c_3 monitored by FTIR difference spectroscopy, two small differences in the IR red-ox spectra were detected at $E_{50\%} = -520$ mV: the shift of the amide I signal from 1656 to 1658 cm^{-1} and the shift of the signal at 1532 cm^{-1} to 1534 cm^{-1}. When the applied potential was lowered, no more changes in the spectra were detected. Thus, applying the potential steps 0 → –520 and –520 → –650 mV, we have obtained two different IR reduced-minus-oxidized (red-ox) spectra corresponding to the electrochemical processes $III_4 \Leftrightarrow III_2II_2$ (Figure 5A) and $III_2II_2 \Leftrightarrow II_4$ (Figure 5B), respectively. They show separately the contributions to the

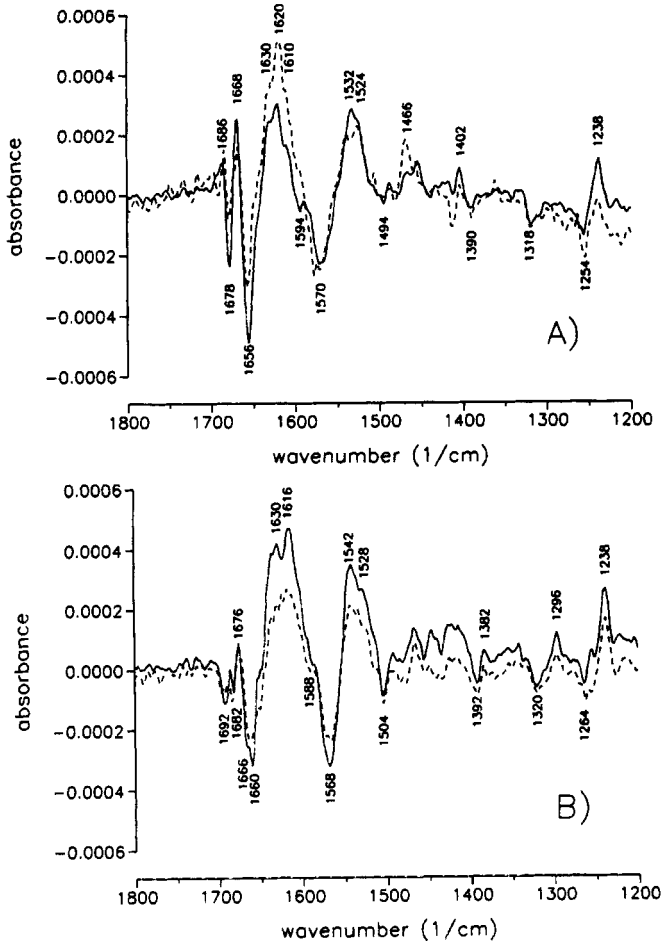

FIGURE 5: FTIR difference spectra of D.d.N. cyt-c_3 in ^1H_2O, pH 7.1 (—), and ^2H_2O, pD 7.5 (- - -), of the intermediate oxidation stages $III_4 \Leftrightarrow III_2II_2$ (A) and $III_2II_2 \Leftrightarrow II_4$ (B).

overall redox-induced conformational change arising from the HP (H_{III}, H_{IV}) and LP hemes (H_I, H_{II}) (Guigliarelli et al., 1990). We shall hereafter term these intermediate states the HP and LP redox states of cyt-c_3.

Parts A and B of Figure 5 show the IR red-ox spectra of the HP and LP redox states, respectively, in ^1H_2O (solid line) ^2H_2O (dotted line). Both spectra, although very similar, show some differences which may reflect specific characteristics of each redox state. The signal at 1692 (–) cm^{-1} belongs to the LP oxidation state spectrum, and the signal at 1686 (+) cm^{-1} belongs to the HP oxidation state.

The signals at 1680 (–)/ 1671 (+) cm^{-1} (overall oxidoreduction process) result from the overlapping of the difference signal specific for HP at 1678 (–)/ 1668 (+) cm^{-1} and the difference signal specific for LP at 1682 (–)/ 1676 (+) cm^{-1}. The amide I signal shifts from 1656 (HP) to 1660 cm^{-1} (LP), suggesting a movement of the only α-helical segment in D.d.N. cyt-c_3 (Val-84 to Lys-101) (Haser et al., 1979) after the reduction of the HP heme pair. The signal at 1668 (+) cm^{-1} in the HP spectrum could be assigned to the amide I C=O stretching mode of β-turns 3_{10} (Krimm & Bandekar, 1986). The second step of the redox-induced overall conformational change thus involves only more flexible segments of the molecule, probably only loops on the molecule surface. Both spectra show a positive signal at 1630 cm^{-1}, which could arise from β-sheet segments.

The strong positive signal at 1618 cm^{-1} seen in the red-ox IR spectra corresponding to the overall redox process results from the overlapping of the signal at 1620 cm^{-1} (HP) and that at 1616 cm^{-1} (LP). The positive signals at 1620/1616 cm^{-1} can arise from the HC=CH stretching mode of aromatic side chains and could be tentatively assigned to phenylalanine residues (Casal et al., 1988; Surewicz et al., 1987). The difference signal at 1610 (+)/1594 (–) cm^{-1} (HP) could arise from the histidine ligands (Venyaminov & Kalnin, 1990).

A large shift is observed in the positive signal at 1532 cm^{-1} (HP) from 1532 to 1542 cm^{-1} (LP). The change of secondary structure involved in both redox transitions could be responsible for this shift. The signals assigned to heme modes remain unchanged in both spectra.

(2.2) D. gigas (D.g) Cytochrome c_3. (2.2.1) Overall Redox Process: Transition from the Fully Oxidized to the Fully Reduced Oxidation State ($III_4 \Leftrightarrow II_4$). Figure 4B shows the IR red-ox difference spectra of D.g. cyt-c_3 at pH 7.1 obtained with the bare gold electrode (the same spectra were obtained with the cystamine–SME) in ^1H_2O (solid line) and ^2H_2O (dotted line) upon application of potential steps between 0 and –600 mV. The only common features between D.d.N. and D.g. cyt-c_3 spectra in ^1H_2O are the signals assigned to heme modes at 1390 (–), 1402 (+), and 1238 (+) cm^{-1}. A summary of the difference IR signals found in the spectra of both cyt-c_3 is shown in Table I. In the amide I region the spectrum shows three strong signals at nearly the same positions as in the D.d.N. red-ox spectrum at 1675 (–), 1652 (+), and 1634 (–) cm^{-1} and a weak positive signal at 1686 cm^{-1}.

A similar estimation of the number of peptide bonds involved in the overall redox-induced conformational change, taking the maximum amplitude of the difference signals *vs* the total amide I absorbance (absorption maximum at 1642 cm^{-1}), yields at most four to five amino acids. In the region of –HC=CH– stretching modes, the spectrum shows only one positive signal of medium amplitude at 1612 cm^{-1} which could arise either from heme modes or from the ring vibration modes of a phenylalanine. According to amino acid sequence of D.g. cyt-c_3, Phe-23 is the only possible candidate (Ambler et al., 1971). For the signals at 1568 (–) and 1542 (+) cm^{-1} and the shoulder at 1594 cm^{-1} we propose the same assignment as for D.d.N. cyt-c_3. The distinct, small, but very sharp positive signal at 1512 cm^{-1} probably arises from the phenol group vibration modes of Tyr-45 and Tyr-68 (Venyaminov & Kalnin, 1990).

Small shifts and intensity changes as compared to ^1H_2O are detected in the spectrum recorded in ^2H_2O (Figure 4B, dotted line). The signals at 1675, 1652, and 1634 cm^{-1} (^1H_2O) shift to 1672, 1650, and 1628 cm^{-1} in ^2H_2O. The negative signal at 1593 cm^{-1} in ^1H_2O appears as a shoulder in ^2H_2O, probably a consequence of the amplitude increase of the 1568-cm^{-1} signal. The positive signal at 1512 cm^{-1} almost disappears in ^2H_2O.

(2.2.2) IR-Detectable Intermediate Oxidation Stages Corresponding to the Bielectronic Redox Processes $III_4 \Leftrightarrow III_2$-$II_2 \Leftrightarrow II_4$. In analogy to D.d.N. cyt-c_3, a reductive titration of D.g. cyt-c_3 monitored in the IR reveals that at $E_{50\%} = -460$ mV there is a shift of the signals at 1674 (–), 1654 (+), 1632 (–), and 1538 (+) cm^{-1} to 1675, 1652, 1634, and 1542 cm^{-1} in the transition from the HP redox state to the fully reduced state ($III_2II_2 \Leftrightarrow II_4$). When the applied potential was lowered, no further changes were detected in the red-ox spectra. Thus, applying potential steps of 0 → –460 and –460 → –600 mV, we have obtained the IR red-ox difference spectra of the HP and LP oxidation states (parts A and B, respectively of Figure 6). Although in this case we also obtained very similar spectra, there are some remarkable differences which may be char-

Table I: Observed Frequencies (cm^{-1}) in the Reduced-Minus-Oxidized IR Difference Spectra of Cytochromes c_3 in ^1H_2O

D.d.N. total	D.d.N. HP	D.d.N. LP	D.g. total	D.g. HP	D.g. LP
		Region of Amide I C=O Stretching Mode			
1692 (–) w		1692 (–) w			
1686 (+) w	1686 (+) w	1682 (–) w	1686 (+) w	1686 (+) w	
1680 (–) m	1678 (–) m	1676 (+) w	1675 (–) vs	1674 (–) vs	1678 (–) vs
1671 (+) w					
	1668 (+) s	1660 (–) s			
1658 (–) vs	1656 (–) vs		1652 (+) vs	1654 (+) vs	1652 (+) vs
					1642 (–) vs
1630 (+) vs	1630 (+) vs	1630 (+) vs	1634 (–) s	1632 (–) s	
		C=C Stretching Region of Aromatic Amino Acid Side Chains			
1618 (+) vs	1620 (+) vs	1616 (+) vs			
	1610 (+) vs		1612 (+) m	1614 (–) m	1610 (+) w
		C—N Stretching Modes, COO^- Antisymmetric Stretching Mode of Ionized Carboxylate Groups, Amide II Modes, and Porphyrin Ring Skeleton Modes			
1568 (–) vs	1570 (–) s	1568 (–) vs	1569 (–) m	1570 (–) m	1566 (–) m
		1542 (+) s	1542 (+) m		1542 (+) m
1534 (+) vs	1532 (+) s			1538 (+) m	
		Tyrosine Phenol Group Vibration Mode			
			1512 (+) m	1512 (+) w	1512 (+) w
		Heme Modes			
1502 (–) w	1494 (–) w	1504 (–) w			1494 (–) w
1404 (+) w	1402 (+) w		1402 (+) w	1402 (+) w	1402 (+) w
1390 (–) w	1390 (–) w	1392 (–) w	1390 (–) w	1390 (–) w	1390 (–) w
1238 (+) s	1238 (+) w	1238 (+) s	1238 (+) s	1238 (–) s	1238 (+) m

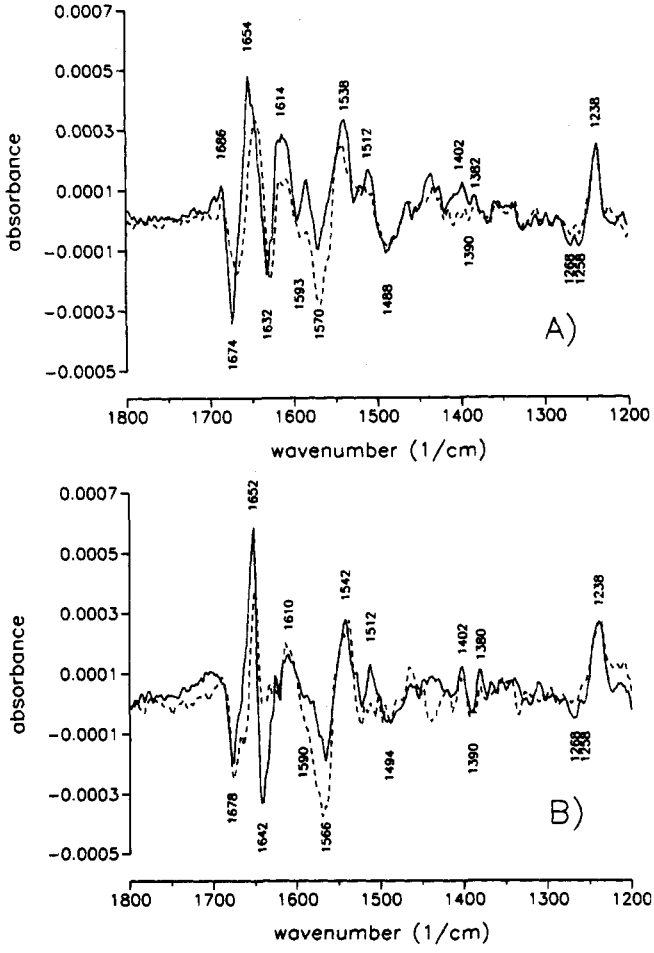

FIGURE 6: FTIR difference spectra of D.g. cyt-c_3 in ^1H_2O, pH 7.1 (—), and ^2H_2O, pD 7.5 (- - -), of the intermediate oxidation stages $III_4 \Leftrightarrow III_2II_2$ (A) and $III_2II_2 \Leftrightarrow II_4$ (B).

acteristic for each oxidation state.

In the amide I region, the band at 1686 (+) cm^{-1} is characteristic for the HP redox state; the signals at 1674 (–), 1654 (+), and 1632 (–) cm^{-1} (HP) shift to 1678 (–), 1652 (+), and 1642 (–) cm^{-1} (LP). According to the variation of amide I absorption with different secondary structures, we tentatively attribute the signals at 1686 and 1678/1674 cm^{-1} to turns, at 1652/1654 cm^{-1} to α-helices, and at 1632 cm^{-1} to β-sheet segments (Krimm & Bandekar, 1986). This would imply a rather different secondary structure content in D.g. cyt-c_3 with respect to D.d.N. cyt-c_3, which is not surprising because of the poor homology of their amino acid sequences (Haser et al., 1979). In the signal at 1686 cm^{-1} we can also expect contributions arising from the symmetric stretching mode of protonated carboxylic groups. However, the signal at 1642 cm^{-1} (LP) disappears completely in the ^2H_2O spectrum, indicating that it does not arise from amide I modes but from some amino acid side-chain absorption. According to its frequency, it could correspond to a $-NH_3^+$ symmetric deformation mode of a protonated lysine.

Since only preliminary X-ray data of the structure of D.g. cyt-c_3 have been published (Sieker et al., 1986), it is difficult to assign the difference IR signals to specific amino acids. However, if we take the spatial arrangement of the four hemes in D.d.N. and D.v.M. cyt-c_3 as a model, we can suggest some possible amino acids as being involved in the redox conformational change. The positive signal at 1614 cm^{-1} (HP) is replaced by a broad structure of weak intensity centered at 1610 cm^{-1} in the LP-state spectrum. We tentatively assign this signal to the only phenylalanine residue (Phe-23) of D.g. cyt-c_3 (Ambler et al., 1971). However, the molecule contains two tyrosine residues (Tyr-45 and Tyr-68); in the spectra of both oxidation states, a sharp signal at 1512 (+)/ 1520 (–) cm^{-1} is detected, which could arise from vibration modes of tyrosine. The fact that this signal disappears in the ^2H_2O spectrum of both oxidation states supports the assumption that these signals arise from vibration modes of protonated phenol groups (Venyaminov & Kalnin, 1990). The signal at 1488 (–) cm^{-1} (HP) could arise from ring vibration modes of Phe-23.

(2.3) Effects of pH on the IR Red-Ox Difference Spectra Corresponding to the Overall Redox Process ($III_4 \Leftrightarrow II_4$) in Both Cytochromes c_3. Preliminary data obtained from IR red-ox difference spectra of D.g. cyt-c_3 recorded at different

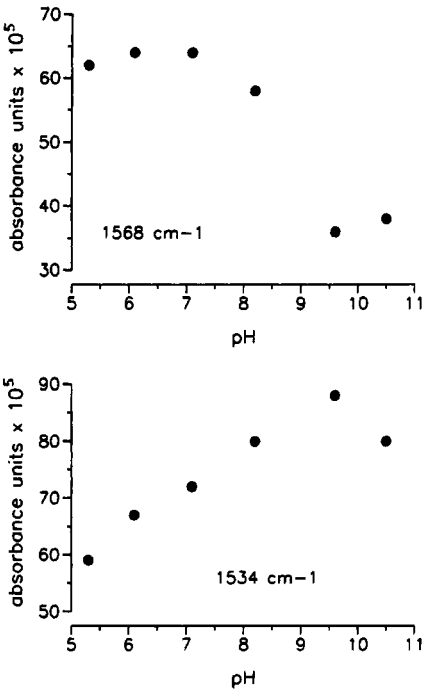

FIGURE 7: pH dependence of the amplitude of the difference signals at 1568 (–) and 1534 (+) cm^{-1} in the IR red-ox spectra of D.d.N. cyt-c_3 corresponding to the overall redox process $III_4 \Leftrightarrow II_4$. Spectra were recorded at 5 °C.

pH values in the range from 6.1 to 11.4 showed very small variance with pH in the amide I spectral region. The 1686-cm^{-1} (HP) signal tends to disappear at alkaline pH, which is in agreement with the assignment of this signal to a protonated heme propionate and suggests that it arises from the highest potential heme. Some small pH effects were also detected for the signals at 1654 cm^{-1} in the HP and at 1642 cm^{-1} in the LP oxidation state difference spectra (data not shown). In contrast to that, a stronger pH dependence in the range from 5.3 to 10.5 was found for D.d.N. cyt-c_3. The predominant pH-dependent spectral changes in the red-ox spectra corresponding to the overall redox process were observed in the difference signal at 1568 (–)/1534 (+) cm^{-1}. The amplitude of the signal at 1568 cm^{-1} remains constant at neutral and slightly acidic pH and strongly decreases at alkaline pH (Figure 7). On the other hand, the amplitude of the signal at 1534 cm^{-1} increases linearly in the range of pH 5.3 to ca. 9.0 and then remains constant at more alkaline pH values (Figure 7). Kitagawa et al. (1977) have found a pH dependence of the Raman signal at 1541 cm^{-1} for ferrocytochrome c_3 from *D. vulgaris*. A more extensive study of the pH dependence of the IR spectral features of D.d.N. and D.g. cyt-c_3 is in progress.

DISCUSSION

(1) Electrochemistry and UV–Vis Difference Spectroscopy. The direct and reversible electrochemistry of various cytochromes c_3 from different *Desulfovibrio* species at bare metallic surfaces is widely established (Bianco & Haladjan, 1979, 1982; Bianco et al., 1979, 1986; Nivière et al., 1988; Hinnen et al., 1983; Hinnen & Niki, 1989; Sagara et al., 1991). Here, we have demonstrated that quantitative and reversible direct electrochemistry of cyt-c_3 in a specifically designed thin-layer electrochemical cell can be combined with UV–vis and FTIR spectroscopic investigations.

The redox potential values which we obtain for D.d.N. cyt-c_3 at the Pys–SMEs are nearly the same as those found by other authors at gold, glassy carbon, and mercury electrodes (Bianco et al., 1979, 1986; Bianco & Haladjan, 1979, 1982). The macroscopic redox potentials obtained from our titration curves, assuming a model with four noninteracting components, are very close to those found by Gayda et al. (1988) on the basis of a model allowing heme–heme interactions.

We have studied the electrochemical behavior of D.g. cyt-c_3 using the bare gold electrode and a cystamine–SME, the latter suitable for negativity charged proteins (Hill & Lawrance, 1989). The titration curves obtained with both electrodes are nearly identical at neutral pH. At alkaline pH, a slight loss of reversibility in the electrochemical process is detected only with the cystamine–SMEs. The titration curves clearly deviate from a Nernstian behavior and are much steeper than they should be in the case of noninteracting redox centers.

The half-wave redox potential obtained from the titration curves at different pH conditions was in every case $E_{50\%}$ = 460 mV. From ESR measurements, Xavier et al. (1979) found two electrochemically indistinguishable HP hemes with E = –445 mV and two LP hemes with redox potentials at –516 and –525 mV.

The cyclic voltammograms do not exhibit a clear dependence of the midpoint redox potentials on pH and show two cathodic processes at –405 and –530 mV and only one anodic process at –450 mV. Using mercury and graphite electrodes, Nivière et al. (1988) obtained cyclic voltammograms in which the separation between the cathodic processes was much higher that between the two observed anodic processes, which were poorly resolved.

The cooperative redox behavior of D.g. cyt-c_3 is thought to be coupled to a proton-linked equilibrium between two tertiary structures (Coletta et al., 1991). However, the difference among the individual heme redox potential values for the acidic and basic forms of D.g. cyt-c_3 is too small too be detected with a conventional titration curve (25 mV for the HP heme pair and 30 and 50 mV for the LP hemes).

The redox titrations monitored by UV–vis difference spectroscopy show small shifts of the α and Soret bands associated with the applied potential value. For both cytochromes, the UV–vis distinguishable hemes show small shifts in the range 1–3 nm of the bands belonging to both oxidation states, thus suggesting very similar local heme environments. However, for D.d.N. cyt-c_3 we were able to separate two HP from two LP hemes in agreement with the results of Cammack et al. (1984), whereas for D.g. cyt-c_3 only the highest redox potential HP heme has a different optical difference spectrum.

Abnormalities in the absorption and CD spectra restricted to the Soret band have been previously reported for an intermediate oxidation stage of D.v.M. cyt-c_3 which corresponds approximately to the half-reduction oxidation state (Tabushi et al., 1983; Yagi et al., 1984).

(2) FTIR Difference Spectroscopy. The total amplitude of the red-ox IR difference spectra corresponding to the overall redox process in both cytochromes ($III_4 \Leftrightarrow II_4$) indicates that the conformational change involved in the redox transition is very small. The same was suggested by Fan et al. (1990) from NMR studies with D.v.M. cyt-c_3. Two red-ox IR difference spectra with nearly the same amplitude were found corresponding to the transitions $III_4 \Leftrightarrow III_2II_2$ and $III_2II_2 \Leftrightarrow II_4$ involving the HP and the LP hemes, respectively, for both cytochromes. We thus conclude that a stable intermediate oxidation state exists, which corresponds to the half-reduction of the molecule as it was found for D.v.M. cyt-c_3 (Tabushi et al., 1983) and D.v.H. cyt-c_3 (Santos et al., 1984). This oxidoreduction pattern suggests that in both molecules the

overall redox process proceeds between two heme pairs which act in a concerted way. In fact, kinetic studies carried out with *D. vulgaris* cyt-c_3 have shown that the reaction rate of the HP heme reduction is considerably faster than that of the LP hemes, suggesting a strong interaction between the HP hemes (Favaudon et al., 1978; Yagi, 1984). The reduced-minus-oxidized (red-ox) IR difference spectra reflect a conformational change in two steps, each one involving half of the whole molecule. According to Colleta et al. (1991), the pH-dependent redox equilibrium in D.g. cyt-c_3 could arise from a structural alteration mostly involving the interdomain interface. A redox-induced conformational change in two steps would rather be compatible with the heme assignment proposed by Guigliarelli et al. (1990), in which H_{III} has the highest redox potential value and H_I belongs to the LP heme pair. The hypothesis that in each step only one domain is involved seems to be attractive.

CONCLUSIONS

The red-ox FTIR difference spectra presented here clearly demonstrate that small but characteristic conformational changes of the protein moiety are associated with the redox transitions of cytochromes c_3. Although crystal structures of a cyt-c_3 in **both** redox states (III_4 and II_4) or in intermediate states are not yet available, this was proposed by other authors (Singleton et al., 1979; Pierrot et al., 1982; Tabushi et al., 1983; Yagi, 1984; Gayda et al., 1987). The individually resolved steps of the redox transition $III_4 \Leftrightarrow III_2II_2$ and III_2-$II_2 \Leftrightarrow II_4$, yielding FTIR difference spectra of similar amplitudies, indicate that the total redox transition proceeds in two concerted steps, each one involving two hemes. On the basis of our analysis of the FTIR difference spectra, we suggest that the main conformational changes affect the interdomain region, as suggested by Coletta et al. (1991) for the pH-dependent redox equilibrium of the D.g. cyt-c_3. We further suggest that these conformational changes give rise to the biphasic reduction kinetics observed for various *Desulfovibrio* cyt-c_3 (Capellière-Blandin et al., 1986; Catarino et al., 1991).

Although the assignment of some of the difference bands to aromatic amino acid side-chain modes is still tentative and is based only on typical group frequencies and deuteration effects, the FTIR data present convincing evidence that changes of conformation or of local environment of aromatic amino acid residues are associated with both intermediate redox transitions for both (D.d.N. and D.g.) cyt-c_3. Furthermore, the spectra clearly indicate the involvement of at least two phenylalanine residues in the overall redox process in D.d.N. cyt-c_3. On the basis of the amino acid sequence of D.g. cyt-c_3 (Ambler et al., 1971), it appears that in this protein the invariant Phe-23 could play the role of a π-conducting amino acid between the high-potential heme pair as does Phe-20 in D.v.M. cyt-c_3 (Higuchi et al., 1984). For the second intermediate reductive transition ($III_2II_2 \Leftrightarrow II_4$) in D.g. cyt-$c_3$, we propose on the basis of our FTIR difference spectra that the π-conducting amino acid function between the low-potential heme pair might be carried out by a tyrosine residue.

ACKNOWLEDGMENT

D.D.S. gratefully acknowledges a postdoctoral fellowship from the Spanish Consejo Superior de Investigaciones Científicas. W.M. is indebted to the Deutsche Forschungsgemeinschaft for financial support (Ma 1054/2-2 and 5-1) and a Heisenberg Fellowship. We are greatly indebted to Prof. K. K. Rao, King's College, London, for his generous supply of protein and to Prof. W. Kreutz, Institut für Biophysik, Freiburg, for encouraging support.

REFERENCES

Ambler, R. P., Bruschi, M., & Le Gall, J. (1971) *FEBS Lett. 18*, 347–350.
Baymann, F., Moss, D., & Mäntele, W. (1991) *Anal. Biochem. 199*, 269–274.
Berthomieu, C., Boussac, A., Mäntele, W., Breton, J., & Nabedryk, E. (1992) *Biochemistry 31*, 11460–11471.
Bianco, P., & Haladjan, J. (1979) *Biochim. Biophys. Acta 545*, 86–93.
Bianco, P., & Haladjan, J. (1981) *Electrochim. Acta 26*, 1001–1004.
Bianco, P., & Haladjan, J. (1982) *J. Electroanal. Chem. 137*, 367–372.
Bianco, P., Fauque, G., & Haladjan, J. (1979) *Bioelectrochem. Bioenerg. 6*, 385–391.
Bianco, P., Haladjan, J., & Bruschi, M. (1986) *Bioelectrochem. Bioenerg. 15*, 57–66.
Bruschi, M., Hatchickian, E. C., Golovleva, L. A., & Le Gall, J. (1977) *J. Bacteriol. 129*, 30–38.
Cammack, R., Fauque, G., Moura, J. J. G., & Le Gall, J. (1984) *Biochim. Biophys. Acta 784*, 68–74.
Capelière-Blandin, C., Guerlesquin, F., & Bruschi, M. (1986) *Biochim. Biophys. Acta 848*, 279–293.
Casal, H. L., Kohler, U., & Mantsch, H. H. (1988) *Biochim. Biophys. Acta 957*, 11–20.
Catarino, T., Coletta, M., Le Gall, J., & Xavier, A. V. (1991) *Eur. J. Biochem. 202*, 1107–1113.
Chirgadze, Y. N., Fedorov, O. V., & Trushina, N. P. (1975) *Biopolymers 14*, 679–694.
Coletta, M., Catarino, T., Le Gall, J., & Xavier, A. V. (1991) *Eur. J. Biochem. 202*, 1101–1106.
DerVartanian, D. V., & Le Gall, J. (1974) *Biochim. Biophys. Acta 346*, 79–99.
di Gleria, K., Hill, H. A. O., Lowe, V. J., & Page, D. J. (1986) *J. Electroanal. Chem. 213*, 333–338.
Dobson, C. M., Hoyle, N. J., Geraldes, F. C., Wright, P. E., Williams, R. J. P., Bruschi, M., & Le Gall, J. (1974) *Nature 249*, 425–429.
Dolla, A., Cambillau, C., Bianco, P., Haladjan, J., & Bruschi, M. (1987) *Biochem. Biophys. Res. Commun. 147*, 818–823.
Fan, K., Akutsu, H., Kiogoku, Y., & Niki, K. (1990) *Biochemistry 29*, 2257–2263.
Favaudon, V., Ferradini, C., Pucheault, J., Gilles, L., & Le Gall, J. (1978) *Biochem. Biophys. Res. Commun. 84*, 435–440.
Gayda, J. P., Yagi, T., Benosman, H., & Bertrand, P. (1987) *FEBS Lett. 217*, 57–61.
Gayda, J. P., Benosman, H., Bertrand, P., More, C., & Asso, M. (1988) *Eur. J. Biochem. 177*, 199–206.
Guigliarelli, B., Bertrand, P., More, C., Haser, R., & Gayda, J. P. (1990) *J. Mol. Biol. 216*, 161–166.
Gunner, M., & Honig, B. (1991) *Proc. Natl. Acad. Sci. U.S.A. 88*, 9151–9155.
Hartshorn, R. T., & Moore, G. R. (1989) *Biochem. J. 258*, 595–598.
Haser, R., Pierrot, M., Frey, M., Payan, F., Astier, J. P., Bruschi, M., & Le Gall, J. (1979) *Nature 282*, 806–810.
Higuchi, Y., Kusunoki, M., Matsuura, Y., Yasuoka, N., & Kakudo, M. (1984) *J. Mol. Biol. 172*, 109–139.
Hill, H. A. O., & Lawrance, G. A. (1989) *J. Electroanal. Chem. 270*, 309–318.
Hinnen, C., & Niki, K. (1989) *J. Electroanal. Chem. 264*, 157–165.
Hinnen, C., Parsons, R., & Niki, K. (1983) *J. Electroanal. Chem. 147*, 329–337.
Kitagawa, T., Kyogoyu, Y., Izuka, T., Ikeda-Saito, M., & Yamanaka, T. (1975) *J. Biochem. 78*, 719–728.
Kitagawa, T., Ozaki, Y., Teraoka, J., Kyogoku, Y., & Yamanaka, T. (1977) *Biochim. Biophys. Acta 494*, 100–114.

Krimm, S., & Bandekar, J. (1986) *Adv. Protein Chem. 38*, 181–367.

Le Gall, J., & Forget, N. (1978) *Methods Enzymol. 53* (part D [59]), 613–634.

Morimoto, Y., Tani, T., Okumura, H., Higuchi, Y., & Yasuoka, N. (1991) *J. Biochem. 110*, 532–540.

Moss, D., Nabedryk, E., Breton, J., & Mäntele, W. (1990) *Eur. J. Biochem. 187*, 565–572.

Nivière, V., Hatchikian, E. C., Bianco, P., & Haladjan, J. (1988) *Biochim. Biophys. Acta 935*, 34–40.

Park, J. S., Enoki, M., Ohbu, A., Fan, K., Niki, K., & Akutsu, H. (1991) *J. Mol. Struct. 242*, 343–353.

Pierrot, M., Haser, R., Frey, M., Payan, F., & Astier, J. P. (1982) *J. Biol. Chem. 257*, 14341–14348.

Postgate, J. R. (1981) in *The sulfate-reducing bacteria*, Cambridge University Press, Cambridge, U.K.

Sagara, T., Nakajima, S., Akutsu, H., Niki, K., & Wilson, G. S. (1991) *J. Electroanal. Chem. 297*, 271–282.

Santos, H., Moura, J. J. G., Moura, I., Le Gall, J., & Xavier, A. V. (1984) *Eur. J. Biochem. 141*, 283–296.

Schlereth, D. D., & Mäntele, W. (1992) *Biochemistry 31*, 7494–7502.

Schlereth, D. D., & Mäntele, W. (1993) *Biochemistry 32*, 1118–1126.

Sieker, L. C., Jensen, L. H., & Le Gall, J. (1986) *FEBS Lett. 5*, 115–117.

Singleton, R., Jr., Campbell, L. L., & Hawkridge, F. M. (1979) *J. Bacteriol. 140*, 893–901.

Stewart, D. E., Le Gall, J., Moura, I., Moura, J. J. G., Peck, H. D., Xavier, A. V., Weiner, P. K., & Wampler, J. E. (1988) *Biochemistry 27*, 2444–2450.

Surewicz, W. K., Szabo, A., & Mantsch, H. H. (1987) *Eur. J. Biochem. 167*, 519–523.

Susi, H., & Byler, D. M. (1987) *Arch. Biochem. Biophys. 248*, 465–469.

Tabushi, I., Nishiya, T., Yagi, T., & Ikokuchi, H. (1983) *J. Biochem. 94*, 1375–1385.

Taniguchi, I., Toyosawa, K., Yamaguchi, H., & Yasukuochi, K. (1982a) *J. Chem. Soc., Chem. Commun.* 1032–1033.

Taniguchi, I., Toyosawa, K., Yamaguchi, H., & Yasukuochi, K. (1982b) *J. Electroanal. Chem. 140*, 187–193.

Tonge, P., Moore, G. R., & Wharton, C. W. (1989) *Biochem. J. 258*, 599–605.

Venyaminov, S. Y., & Kalnin, M. N. (1990) *Biopolymers 30*, 1243–1257.

Xavier, A. V., Moura, J. J. G., Le Gall, J., & DerVartanian, D. V. (1979) *Biochimie 61*, 689–695.

Yagi, T. (1984) *Biochim. Biophys. Acta 767*, 288–294.

Yagi, T., & Maruyama, K. (1971) *Biochim. Biophys. Acta 243*, 214–224.